Dynamical effects in the formation of magic cluster structures

Francesca Baletto,[1,2] Arnaldo Rapallo,[3] Giulia Rossi,[1] and Riccardo Ferrando[1]
[1]*INFM and IMEM/CNR, Dipartimento di Fisica, Università di Genova, via Dodecaneso 33, I-16146 Genova, Italy*
[2]*ICTP, The Abdus Salam International Center of Theoretical Physics, Strada Costiera 11, I-34014 Trieste, Italy*
[3]*ISMAC/CNR, Via Bassini 15, I-20133 Milano, Italy*
(Received 19 February 2004; published 30 June 2004)

The interplay of energetic, thermodynamic, and kinetic factors is of fundamental importance in the formation of magic structures in nano-objects. Here we combine different kinds of calculations and simulations to determine quantitatively all these factors, and present a thorough study of two paradigmatic examples, the Ag_{38} and Cu_{38} nanoclusters, modeled by a many-body potential interaction. These examples are chosen in order to show that, already in quite simple nano-objects, the formation process is sensitive to all these factors due to the finite size of the systems and to the finiteness of their formation time scale. Both Ag_{38} and Cu_{38} present the capability of retaining memory of the structures assumed during their formation process, here reproduced by freezing and growth simulations. This memory effect can thus strongly influence experimental clusters production, leading to the identification of magic structures that often do not coincide with the minimum potential energy structures located by global optimization techniques.

DOI: 10.1103/PhysRevB.69.235421 PACS number(s): 61.46.+w, 36.40.Ei, 36.40.Sx

I. INTRODUCTION

In the last years there has been an explosive development of nanoscience, which extends to physics, chemistry, biology, and engineering, ranging from basic science to a variety of technological applications, for which the name nanotechnology is often employed. The main purpose of nanoscience is to understand and then to manipulate objects of a few nanometer size (say 1–100 nm). The properties of these nano-objects are qualitatively different from the ones of their constituent parts (being either atoms or molecules) and from those of macroscopic pieces of matter; in particular their properties can vary dramatically with their size. This opens the possibility of a fine tuning of their chemical and physical properties, which can, however, be reached only by controlling precisely the formation process of the nano-objects. Therefore, a fundamental issue in nanoscience is to predict and control the structures of nano-objects depending on their size. In many cases of experimental interest, some specific structures are produced with very high probability, so that they are often named "magic" structures. The concept of a magic structure is indeed one of the most commonly employed and naively defined concepts of nanoscience. A true definition does not exist, and magic structures are usually determined taking into account only geometric and energetic factors, and assuming that these factors can identify the structures which are most frequently produced and observed in experiments. In the case of nanoclusters, well-known examples of magic structures are related to the closing of electronic shells,[1–3] as in the case of small sodium clusters, or to the completion of geometric shells in icosahedra, decahedra, or other polyhedra.[4] Generally speaking, magic structures are believed to reflect the properties of the global minimum of their potential energy surface (PES). The search for global minima has thus motivated a huge amount of work on many different systems, ranging from nanoclusters to proteins and peptides.[5–9] However, as we shall show here, the knowledge of the global minima is not sufficient to determine the structures that are produced with the highest probability. In fact, the most frequently produced structures in experimental conditions can be the result of a complex dynamical interplay of energetic, thermodynamic and kinetic (ETK) effects. This is true already for quite simple nanosystems, such as free metallic clusters of a few tens of atoms studied on typical experimental time scales. Finite-temperature entropic effects can change the relative stability of the global minimum with respect to other low-lying minima, while kinetic effects can cause trapping in long-lifetime metastable structures.

To give a clear demonstration of this point, we propose a procedure which combines different simulation methods and calculations for studying the interplay of ETK effects in the formation of nanoclusters. Our procedure consists of four steps.

(a) Search for the global minimum and all other significant minima of the PES by global optimization algorithms.

(b) Calculation of the equilibrium probabilities of the minima depending on temperature within the harmonic superposition approximation.

(c) Simulation of cluster formation processes (solid state growth [10] and nanodroplet freezing[11]) by molecular dynamics (MD) on realistic time scales.

(d) Comparison of the structures formed in the MD simulations with the equilibrium probabilities.

The above procedure is applied to two simple and paradigmatic examples, such as the metallic nanoclusters of silver (Ag_{38}) and copper (Cu_{38}) at $N=38$ atoms, which is a geometrical magic size for these nanoclusters because it gives the right number of atoms to form a highly symmetric piece of fcc bulk matter [the perfect truncated octahedron (TO) reported in Fig. 1]. Moreover, this is known to be a magic size for silver and copper clusters,[12] if magicity is determined on the basis of energetic considerations only. This can be seen calculating the energy of the global minimum E_{GM} as a function of the cluster size N and plotting the quantity $\Delta_2 E(N)$ (Refs. 12 and 13)

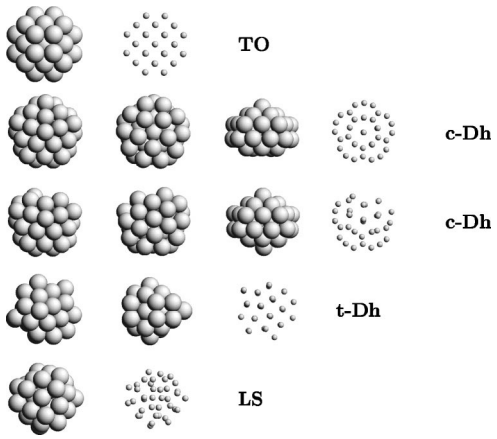

FIG. 1. Global optimization results for Ag_{38} and Cu_{38}. In each row, the same structure is presented in different perspectives and representations. The global minimum is a truncated octahedron (TO) in both cases, followed by two capped decahedra (*c*-Dh). Other possible structures are the asymmetric truncated decahedra (*t*-Dh), which are higher in energy but are closely related to the global minima of silver clusters at sizes just below 38. Finally, low-symmetry (LS) structures are close in energy to the *c*-Dh in the case of silver, and much less favourable in the case of copper. With the exception of the TO, all other structures present local fivefold symmetry points, being thus noncrystalline.

$$\Delta_2 E(N) = -2E_{\mathrm{GM}}(N) + E_{\mathrm{GM}}(N-1) + E_{\mathrm{GM}}(N+1), \quad (1)$$

which measures the relative stability of a cluster of size N with respect to nearby sizes. $\Delta_2 E(N)$ show a well defined maximum at $N=38$ for both Ag and Cu clusters (see Fig. 2). Even though Ag_{38} and Cu_{38} look quite similar, and have the same global minimum structure, their behavior will present significant differences, and they will form different magic structures in the same kind of conditions.

The paper is divided as follows. In Sec. II we illustrate the energetic model for Ag and Cu and our combination of simulation methods and calculations. Section III contains the results and Sec. IV the conclusions.

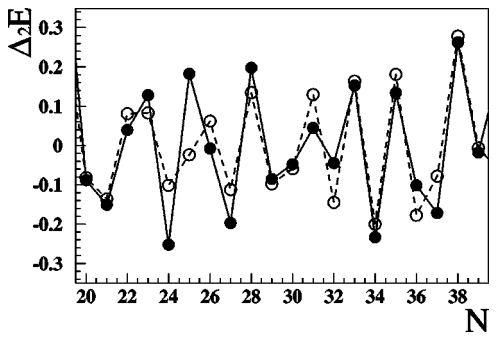

FIG. 2. $\Delta_2 E(N)$ (in eV) for Ag (open circles) and Cu (full circles) clusters. The lines are only guides to the eyes. In both cases, the highest maximum, namely the most stable structure from the energetic point of view, is at $N=38$. Other stable structures are found at $N=33$ and 35.

II. METHOD

In all our simulations, Ag and Cu have been modeled by many-body potentials proposed by Rosato, Guillopé, and Legrand,[14] successfully tested against the properties of nanoclusters and crystal surfaces.[15,16] In this framework, the band energy E_b^i for a given atom i is proportional to the square root of the second moment of the local density of states. E_b^i is an attractive many-body term, the stability is insured by adding a phenomenological core-repulsion term E_r^i of the Born-Mayer type. The potential energy of atom i is given by

$$E_c^i = E_b^i + E_r^i, \quad (2)$$

where the band energy is

$$E_b^i = -\left(\sum_{j, r_{ij} < r_c} \xi^2 \exp\left[-2q\left(\frac{r_{ij}}{r_0} - 1 \right) \right] \right)^{1/2} \quad (3)$$

and the repulsive term is

$$E_r^i = \sum_{j, r_{ij} < r_c} A \exp\left[-p\left(\frac{r_{ij}}{r_0} - 1 \right) \right]. \quad (4)$$

The parameters (ξ, A, p, q) are fitted on bulk properties of the crystal, and they are reported in Ref. 17.

As stated in the Introduction, the first step of our calculations is the search for the global minimum, and of the other low-lying minima. This task is accomplished by genetic algorithm optimization,[7] whose results are checked by quenching $\sim 10^6$ configurations obtained in long (on the scale of 10 μs) MD runs at high temperature. Thus, a huge catalog of minima is collected and we single out the most significant ones for defining the energy landscape.

After having found the minima, we calculate their equilibrium probabilities depending on temperature in the harmonic superposition approximation (HSA).[18,19] The HSA expresses configurational part Q of the partition function as a sum of integrals Q_i localized around each minimum i on the PES. Each Q_i is then calculated in harmonic approximation. Thus, the equilibrium probability p_i is written as

$$p_i = \frac{Q_i}{Q} \simeq K \frac{1}{h_i} \left(\prod_{k=1}^{3N-6} \omega_{ik} \right)^{-1} \exp\left(-\frac{E_i}{k_B T} \right), \quad (5)$$

where E_i, ω_{ik}, and h_i are the energy, the eigenfrequencies and the group order of minimum i, N is the cluster size, k_B is the Boltzmann constant, and K is a normalization constant.

The third step is the MD simulation of cluster formation processes in realistic conditions, taking inspiration from experimental procedures. Various methods have been developed to prepare noble-metal particles in the laboratory.[2] These include for example condensation of a metallic vapor on different substrates and nucleation in an inert-gas atmosphere. In particular, in the latter case [inert gas aggregation (IGA) sources[2,20–22]] the warm metal vapor is thermalized by an inert gas (for example helium or argon) at room temperature which causes the formation of particles (seeds); then the seeded beam is detected by electron diffraction in order to have direct information about the structures while clusters are still in flight. To take into account the kinetics, we implement two models to simulate the cluster formation process

on the realistic time scale, namely, the freezing of liquid nanodroplets and the cluster growth from a small initial seed.[10,11] These models are intended to mimic the formation of free nanoclusters in an inert gas atmosphere, where the cold inert gas flows through the hot metallic vapor causing the supersaturation and the clustering of the metallic atoms. In more detail, the freezing simulations mimic those conditions where clustering takes place at such high temperature, so that the clusters grow as liquid droplets and are cooled down only after growth is completed. In this case, the final structure of the cluster is determined by the cooling process that takes place at constant number of atoms. Our freezing simulations start at 700 K (at this temperature Ag_{38} and Cu_{38} are liquid, since small clusters melt at considerably lower temperatures than bulk matter[23]) and cool down to 200 K at a rate of 1 K/ns, comparable to the one estimated from experiments.[11,20] The growth simulations mimic those situations where the clusters are grown in a cooler inert gas atmosphere, so that they can become solid while they are still growing. In this case the final structure of the cluster is determined by the growth process itself. The growth simulations start from a small seed of 7 atoms; further atoms are deposited one by one[2] at a time interval of 100 ns, keeping the temperature constant. Simulations are stopped after having reached the desired size and let the cluster evolve for further 100 ns. The final step is the comparison of the frequencies f of the most important minima, as observed after quenching down thousands of snapshots taken in the freezing and in the growth simulations, with their equilibrium probabilities p.

III. RESULTS

A. Global optimization results

We have searched for the global minima of Ag and Cu clusters in the size range $20 \leqslant N \leqslant 40$, in order to build up the minimum energy sequence of Fig. 2, and made a thorough analysis at $N=38$ to single out all the significant minima having a non-negligible probability of being occupied in the temperature range of the MD simulations.

The most significant minima at $N=38$ are shown in Fig. 1. As shown in Refs. 15, 17, and 19, for both Ag_{38} and Cu_{38}, the GM is the TO structure. This is the only significant crystalline structure. In fact, all other low-lying minima present at least one local fivefold symmetry point, so that they cannot be considered as pieces of bulk lattice. It is known that noncrystalline structures such as decahedra and icosahedra[4] are often the global minima of small clusters (see, for example, Refs. 15, 19, and 24). In our case, there is a series of noncrystalline structures after the TO. The next few minima (see Fig. 1) above the TO are capped decahedra (c-Dh), based on the decahedron of 23 atoms, covered by a further layer arranged in such a way that it breaks the perfect arrangement in columns of the decahedral structure. The second-lowest minimum (of C_{5v} group symmetry) is indeed a 23 decahedron capped by five three-atom islands on hcp stacking,[25] and stays about 0.19 and 0.15 eV higher than the TO in Ag and Cu, respectively. Other defected decahedral structures are asymmetric truncated decahedra (t-Dh),[4] which are fragments of the complete decahedron (a pentagonal bipyramid) of 54 atoms. The t-Dh structures preserve the arrangement in columns of decahedral structures. Even though these t-Dh structures are considerably higher in energy than the previous ones, they will play an important role in the clusters growth. Finally, we find a low-symmetry (LS) structure, that closely resembles the chiral disordered global minimum found in Au_{38},[26] and which is close in energy to the c-Dh structures in Ag_{38}, and somewhat higher in Cu_{38}.

The results at $N<38$ are important to discuss the results of the growth simulations (see the following). The main point is that in the range $30<N<37$ all global minima belong to the decahedral motif for both Ag and Cu, with the single exception of Cu_{37} which is a defected fcc structure. As can be seen from the maxima of $\Delta_2 E(N)$ in Fig. 2, both metals present clusters of good energetic stability at $N=33$ and 35. In Ag, the global minima at these sizes are fragments of the 38 atoms t-Dh shown in Fig. 1, while in Cu the global minima are fragments of the c-Dh structures at $N=38$.

B. Freezing simulations

In the freezing simulations (Figs. 3 and 4), three regimes are identified depending on temperature. At high T ($T>400$ K in Ag and $T>450$ K in Cu), clusters behave clearly as liquid droplets, fluctuating fast among a huge number of minima. The occupation probability of the global minimum, and of the other low-lying minima in general, is small, and no magic structure can be singled out. At intermediate temperatures ($300<T<400$ K in Ag and $300<T<450$ K in Cu), a few minima are likely to be occupied. These minima are TO, c-Dh and LS structures, as listed in Fig. 1. The clusters are fluctuating among them, however, on a slower time scale than at high temperature. In the intermediate temperature range, Ag_{38} and Cu_{38} behave differently. In Ag_{38}, the most likely structures are the c-Dh and the LS, essentially with the same frequency. On the contrary, in Cu_{38}, a single structural motif (the c-Dh) is clearly preferred, so that there is an intermediate-temperature regime where the magic structure does not coincide with the lowest-energy one. These results are due to thermodynamic (free-energy) effects. In fact, calculating the equilibrium probabilities of the different structures p_{TO}, $p_{c\text{-Dh}}$, and p_{LS}, making the ratios $r_{\mathrm{TO}}=p_{\mathrm{TO}}/(p_{\mathrm{TO}}+p_{c\text{-Dh}}+p_{\mathrm{LS}})$, $r_{c\text{-Dh}}=p_{c\text{-Dh}}/(p_{\mathrm{TO}}+p_{c\text{-Dh}}+p_{\mathrm{LS}})$, and $r_{\mathrm{LS}}=p_{\mathrm{LS}}/(p_{\mathrm{TO}}+p_{c\text{-Dh}}+p_{\mathrm{LS}})$, and comparing them with the corresponding ratios of the frequencies f observed in the simulations, we obtain a good agreement both at high and intermediate temperatures (see Figs. 3 and 4). Our findings thus show a structural transformation at intermediate temperature, which has some analogy with the observation of icosahedral precursors to the melting of TO gold clusters in MD simulations.[27] At lower temperatures ($T<300$ K) the most frequently observed structures pertain to the global minimum. However, in about 10–20% of the cases, the low-temperature structure is a c-Dh, and this causes a discrepancy between the observed frequencies and the equilibrium probabilities, indicating that the low-temperature c-Dh are nonequilibrium structures, due to a kinetic trapping effect[10,28] into the structures which are the most likely ones

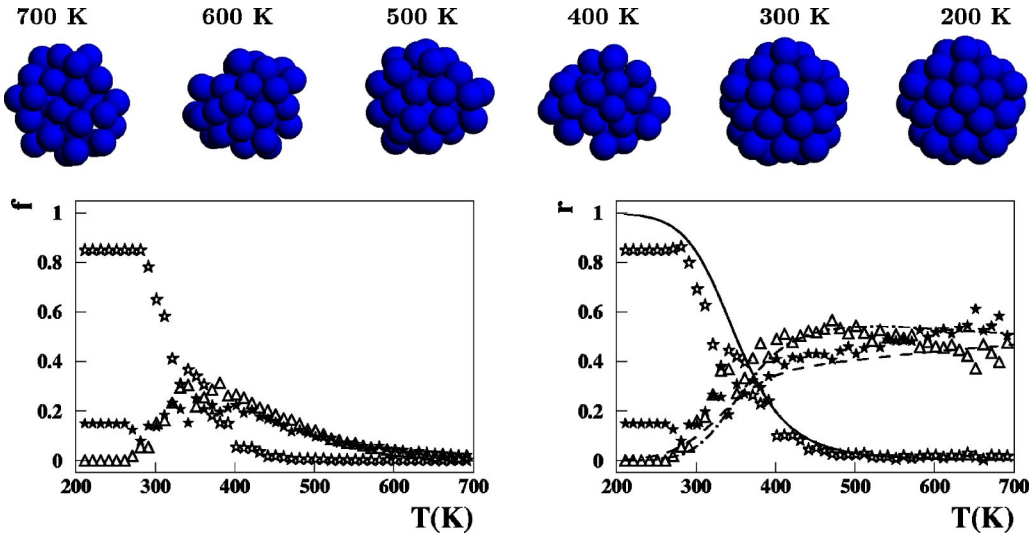

FIG. 3. Results of the freezing simulations of Ag_{38}, and comparison with the equilibrium probabilities. In the first row, snapshots from a freezing simulation are reported. Starting from $T=700$ K, the cluster is cooled down to 200 K at a rate of 1 K/ns. Above 400 K the cluster fluctuates fast among many different isomers. In between 400 and 300 K, the cluster presents a *c*-Dh structure, and stays kinetically trapped into this structure down to low temperature. In the left and right panels the open stars, the full stars and the triangles refer to the TO, *c*-Dh, and LS structures, respectively. In the left panel, the relative frequencies $f_{TO}, f_{c\text{-}Dh}, f_{LS}$ of the different structures are reported. In the right panel, the ratios among equilibrium probabilities r_{TO}, $r_{c\text{-}Dh}$, and r_{LS} (full, dashed, and dash-dotted lines) are reported and compared to the corresponding ratios of the frequencies observed in the freezing simulations (symbols). Down to intermediate temperatures, equilibrium probabilities and freezing results agree well, indicating that *c*-Dh and LS structures are in close competition. At low temperatures, the global-minimum TO structure prevails, but the discrepancy between equilibrium probabilities and freezing results indicate the occurrence of some kinetic trapping into *c*-Dh structures.

at higher temperatures. The low-temperature structures thus may retain some memory of the structures encountered at higher temperatures. This happens also for such small system on rather slow time scales.

C. Growth simulations

An even more complex interplay of thermodynamic and kinetic effects takes place in the growth simulations (Figs. 5

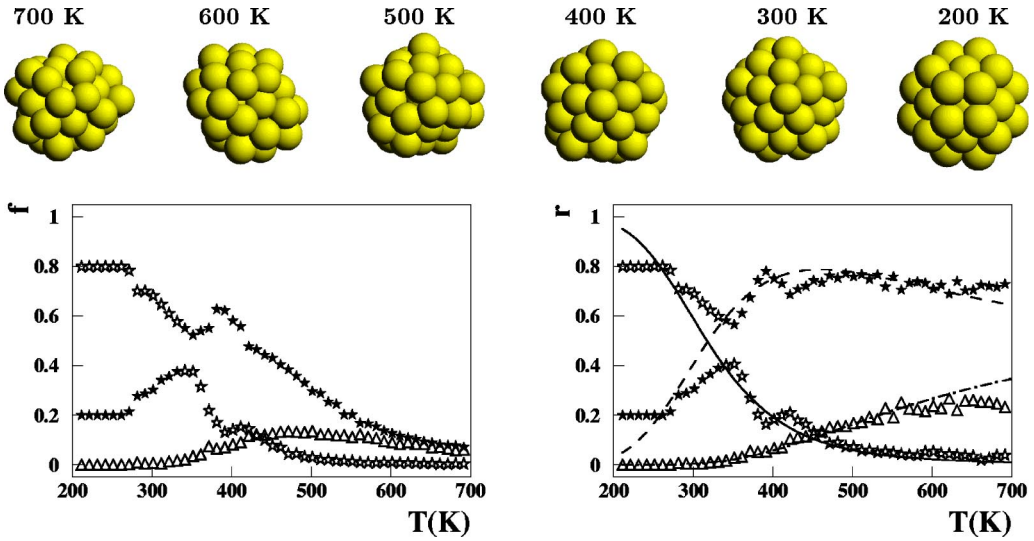

FIG. 4. As in Fig. 3, but in the case of Cu_{38}. In the snapshots of the first row, the cluster presents a *c*-Dh structure at 400 and 300 K, but finally solidifies into the global-minimum TO structure. In general, at intermediate temperatures, *c*-Dh structures clearly prevail, while LS structures always have a low frequency (see the left panel). TO structures are again dominating at low temperatures. The ratios in the right panel show a good coincidence between freezing results and equilibrium probabilities down to intermediate temperatures, and some kinetic trapping into *c*-Dh structures at low temperatures.

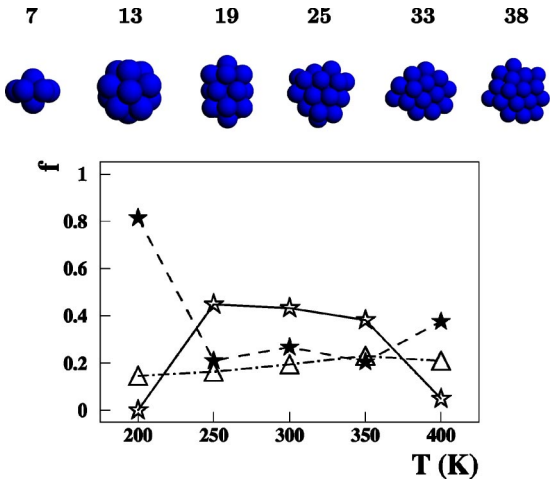

FIG. 5. Ag growth simulations results. In the top row, snapshots from a simulation at $T=200$ K are reported at different sizes. The structures of the snapshots pertain to the global minima up to $N=33$; then growth is kinetically trapped into defected *t*-Dh structures, which are neither energetically nor entropically favorable. The graph reports the structural frequencies f_{TO}, f_{Dh}, f_{LS} of the TO, *c*-Dh, plus *t*-Dh, and LS structures (open stars, full stars, and triangles, respectively), at $N=38$ and at different growth temperatures. The lines are only guides to the eyes. At low temperatures, strong kinetic trapping into *t*-Dh structures occur. This is followed by and intermediate temperature regime where the three structural motifs are essentially equally likely. At high temperatures, entropic effects favor *c*-Dh and LS structures at expense of the TO.

and 6). In this case, we perform several simulations at $T=200$, 250, 300, 350, and 400 K, and observe the structures obtained at size 38. At 200–250 K, kinetic trapping into either *c*-Dh or *t*-Dh structures is the fate of essentially all

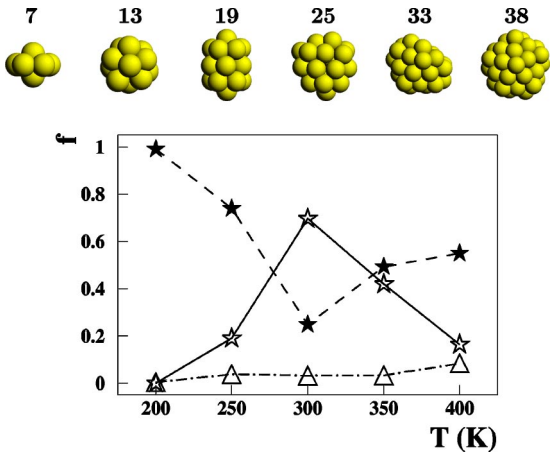

FIG. 6. Cu growth simulations results. In the top row, snapshots from a Cu simulation at $T=400$ K are reported. Again, the snapshots reproduce the global minima up to $N=33$, but the growth structure at $N=38$ is not the global minimum but a *c*-Dh, which is entropically favored at this temperature. Around 200 K, there is a strong kinetic trapping into *c*-Dh structures formed at smaller sizes. At intermediate temperatures the TO structure is preferentially grown; at high *T*, *c*-Dh structures again prevail due to entropic effects.

simulations, so that the *magic* structure never coincides with the global minimum, which is also the free-energy minimum in this temperature range. This kinetic trapping is due to the fact that the global minima at sizes 30–37 atoms are either *t*-Dh or *c*-Dh (with the single exception of Cu_{37}). Thus the clusters retain a strong memory of the structures encountered at smaller sizes. At 300–350 K, kinetic trapping becomes less effective, even if it is still somewhat present. In this range, the TO structures are still quite likely at equilibrium, and they are indeed observed, together with the *t*-Dh, the *c*-Dh and the LS. Above 350 K, again the *c*-Dh structures prevail in Cu_{38}, as at low temperature. However, the formation of *c*-Dh structures in Cu_{38} above 350 K is not due to kinetic trapping, but to the fact that at these temperatures, the cluster is able, with a good approximation, to reach equilibrium, and to form the most likely equilibrium structures, namely, the *c*-Dh. This is the same entropic effect found in the freezing simulations. In Ag_{38}, the structures at $T>350$ K are either *c*-Dh or LS, again in agreement with the equilibrium calculations. As a final comment, we can observe that in the case of growth, *magic* structures are seldom coinciding with the lowest-energy ones, which are indeed produced with non-negligible frequency only in a rather narrow temperature range.

IV. CONCLUSIONS

In summary, our work clearly shows that the observed cluster structures can derive from a complex dynamical interplay of energetic, thermodynamic, and kinetic (ETK) effects. Kinetic trapping retains the memory of structures of special thermodynamic stability, which are encountered during the evolution or formation of the nano-object. The combination of simulations and calculations that we have proposed here allows us to take into account all ETK effects, thus giving the possibility to understand the structural transformations of nano-objects. In this way we have achieved a clear demonstration of the importance of the dynamical memory in the formation of nano-objects. In fact, already in very small and simple systems, such as metallic clusters of a few tens of atoms, the structural stability is ruled by thermodynamic and kinetic effects rather than purely energetic ones. In fact, for Cu_{38}, decahedral structures are of considerable thermodynamic stability in the intermediate-temperature range due to entropic effects. In the freezing simulations, these structures are very likely to be formed, and then preserved, in some cases, down to low temperatures. On the other hand, decahedral structures are also energetically favorable at sizes just below 38. In the low-temperature growth simulations, it is very likely that the clusters reach these decahedral structures which are then conserved also at larger sizes. In fact, the relaxation towards equilibrium becomes on average slower and slower as the system size grows,[29] so that at a given temperature, a growing cluster can rearrange to the equilibrium shape when its size is small, and then be unable to reach equilibrium when its size is increased. Kinetic trapping is thus a very common phenomenon in the formation of nano-objects. A remarkable example is the ubiquitous experimental observation (in very different systems such as clusters

of Ag and Au atoms, and of C_{60} molecules[20,21,30]) of large icosahedral clusters, at sizes where these structures are energetically and thermodynamically unfavorable. These large icosahedra are formed either by shell-by-shell growth on smaller and energetically favorable icosahedra, or by a solid state transformation of small decahedra into larger icosahedra.[28,31]

ETK effects are expected thus to be important in many cluster systems, and the examples shown here are not to be considered as exceptional ones. In the growth of nanoclusters, kinetic trapping can be expected when the most stable structural motifs change with size, and this is a very frequent situation. On the other hand, in the freezing of nanodroplets, kinetic trapping effects are certainly enhanced in systems with a multiple-funnel PES as the 38-atom cluster. But this is not the only case: preliminary results in the simulation of icosahedral platinum clusters at size 55 show an entropy-driven transformation into amorphized icosahedral-like structures with increasing temperature, and kinetic trapping in these structures during the freezing simulations. Finally, we note that kinetic memory should not be peculiar of nanocluster formation processes, since they are likely to play an important role in several growth, folding, and conformational transition processes in the nanoscale regime.

[1] W. D. Knight, K. Clemenger, W. A. D. Heer, W. A. Saunders, M. Y. Chou, and M. L. Cohen, Phys. Rev. Lett. **52**, 2141 (1984).
[2] W. A. DeHeer, Rev. Mod. Phys. **65**, 611 (1993).
[3] R. L. Johnston, *Atomic and Molecular Clusters* (Taylor and Francis, London, 2002).
[4] T. P. Martin, Phys. Rep. **273**, 199 (1996).
[5] D. J. Wales and H. A. Scheraga, Science **285**, 1368 (1999).
[6] B. Hartke, Angew. Chem., Int. Ed. **41**, 1468 (2002).
[7] R. L. Johnston, J. Chem. Soc. Dalton Trans. **2003**, 4193 (2003).
[8] J. E. Shea and C. L. Brooks, Annu. Rev. Phys. Chem. **52**, 499 (2001).
[9] U. H. E. Hansmann and L. T. Wille, Phys. Rev. Lett. **88**, 068105 (2002).
[10] F. Baletto, C. Mottet, and R. Ferrando, Phys. Rev. Lett. **84**, 5544 (2000).
[11] F. Baletto, C. Mottet, and R. Ferrando, Chem. Phys. Lett. **354**, 82 (2002).
[12] J. P. K. Doye and D. J. Wales, New J. Chem. **22**, 733 (1997).
[13] K. Clemenger, Phys. Rev. B **32**, 1359 (1985).
[14] V. Rosato, M. Guillopé, and B. Legrand, Philos. Mag. A **59**, 321 (1989).
[15] K. Michaelian, N. Rendon, and I. L. Garzon, Phys. Rev. B **60**, 2000 (1999).
[16] T. Ala-Nissila, R. Ferrando, and S. C. Ying, Adv. Phys. **51**, 949 (2002).
[17] F. Baletto, R. Ferrando, A. Fortunelli, F. Montalenti, and C. Mottet, J. Comput. Phys. **116**, 3856 (2002).
[18] D. J. Wales, J. P. K. Doye, M. A. Miller, P. N. Mortenson, and T. R. Walsh, Adv. Chem. Phys. **111**, 1 (2000).
[19] J. P. K. Doye and F. Calvo, Phys. Rev. Lett. **86**, 3570 (2001).
[20] K. Koga and K. Sugawara, Surf. Sci. **529**, 23 (2003).
[21] D. Reinhard, B. D. Hall, D. Ugarte, and R. Monot, Phys. Rev. B **55**, 7868 (1997).
[22] D. Reinhard, B. D. Hall, P. Berthoud, S. Valkealahti, and R. Monot, Phys. Rev. Lett. **79**, 1459 (1997).
[23] M. Schmidt, R. Kusche, B. von Issendorf, and H. Haberland, Nature (London) **395**, 238 (1998).
[24] C. L. Cleveland, U. Landman, T. G. Schaaff, M. N. Shafigullin, P. W. Stephens, and R. L. Whetten, Phys. Rev. Lett. **79**, 1873 (1997).
[25] F. Baletto and R. Ferrando, Surf. Sci. **490**, 361 (2001).
[26] I. L. Garzon, K. Michaelian, M. R. Beltran, A. Posada-Amarillas, P. Ordejon, E. Artacho, D. Sanchez-Portal, and J. M. Soler, Phys. Rev. Lett. **81**, 1600 (1998).
[27] C. L. Cleveland, W. D. Luedtke, and U. Landman, Phys. Rev. Lett. **81**, 2036 (1998).
[28] F. Baletto, J. P. K. Doye, and R. Ferrando, Phys. Rev. Lett. **88**, 075503 (2002).
[29] N. Combe, P. Jensen, and A. Pimpinelli, Phys. Rev. Lett. **85**, 110 (2000).
[30] W. Branz, N. Malinowski, A. Enders, and T. P. Martin, Phys. Rev. B **66**, 094107 (2002).
[31] F. Baletto, C. Mottet, and R. Ferrando, Phys. Rev. B **63**, 155408 (2001).